CHAPTER-4

SYNTHESIS AND MICROSTRUCTURAL CHARACTERIZATION OF Al-Mg_2Si FUNCTIONALLY GRADED COMPOSITES

4.1 Introduction

The microstrucural characterization of fabricated FG-Composites has been presented in this chapter. The chapter includes the results and interpretations of chemical compositions of the base Al alloy and synthesized FG composites, XRD analysis for phase identification, Microstructural features observed under optical microscope, Scanning Electron Microscope and Transmission Electron Microscope. The effects of solidification rate and secondary dendrite arm spacing have been correlated with size, shape and distributions and volume fractions of phase constituents along the radial cross-sectional direction. Fe-intermetallic phases such as π and β phases, Pseudo-binary phases (Chinese script) have been characterized.

4.2 Analysis of chemical composition

The chemical composition of the base alloy and composites (Table 4.1) were analyzed with an Optical Emission Spectrometer (Foundry Master). The reported analyses are average values of at least three sparkings at different locations of the samples.

4.3 X-Ray Diffraction (XRD) analysis

The analysis of XRD pattern from the as-cast FGM specimens of A356 base alloy, FG composites with additions of 2.5, 5, 7.5 and 10 wt.%Mg are shown in Fig. 4.1 and Fig.4.2 shows the XRD pattern of extracted Mg_2Si particles.

Table 4.1 Chemical composition of alloys/FGMs

Alloy/composites	Chemical composition [wt.%]				
	Si	Mg	Cu	Fe	Al
A356 Alloy	7.30	0.30	0.60	0.81	Bal.
A356+2.5 Mg composite	5.48	2.45	0.63	0.55	Bal.
A356+5.0 Mg composite	4.48	5.13	0.61	0.59	Bal.
A356+7.5 Mg composites	5.54	7.50	0.56	0.77	Bal.
A356+10.0 Mg composite	5.54	10.5	0.64	0.78	Bal.

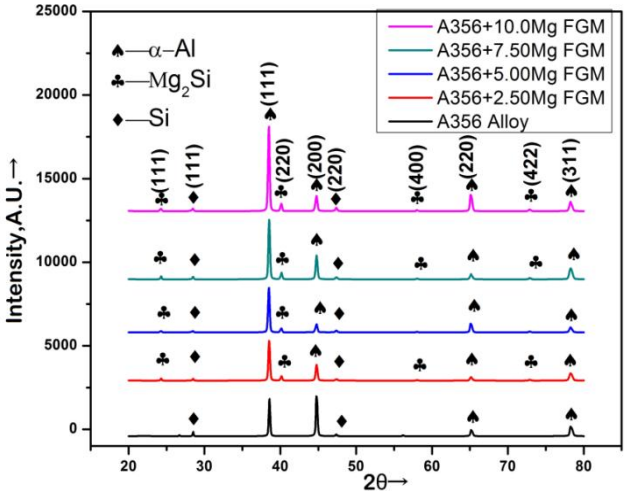

Fig 4.1 XRD Pattern of A356 alloy, A356+2.5Mg, A356+5.0Mg, A356+7.5Mg and A356+10Mg FGMs

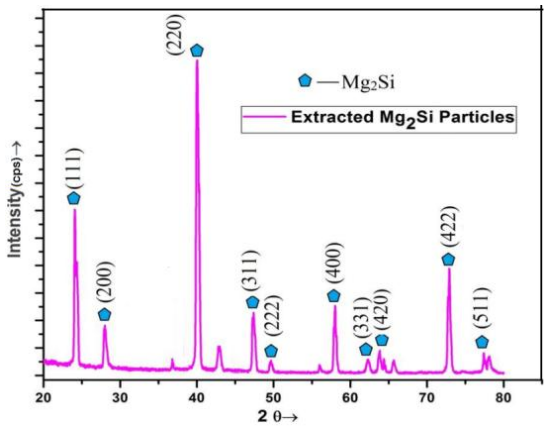

Fig 4.2 XRD Pattern of extracted Mg_2Si particles

The XRD patterns reveals three phases namely α-Al, Mg_2Si, and Si in the four composites fabricated and α-Al and Si in the base A356 alloy. This is in conformity with the as-cast FGM microstructure illustrated in Figs. 4.3-4.7. However, Al-Fe-Si intermetallics are not detected in XRD analysis probably due to their small percentage in the composites. These intermetallic phases could only be detected by scanning electron microscopy.

4.4 Microstructural features in as-cast conditions

Microstructures were observed in three distinct zones along the radial direction of FGMs tubes namely, inner zone, middle transition zone and the outer zone near the mold wall. Figs. 4.3.-4.9 show the typical optical and scanning electron micrographs of different zones of the base alloy and the composites with varying Mg wt.%. The base alloy A356 microstructure exhibits α-Al and Al-Si eutectic (Fig. 4.3), the dendrites are fragmented at outer zones and refined dendrites were observed at the inner zone. The outer zone eutectic Si is highly refined, and gradual coarsening is discerned towards inner zone.

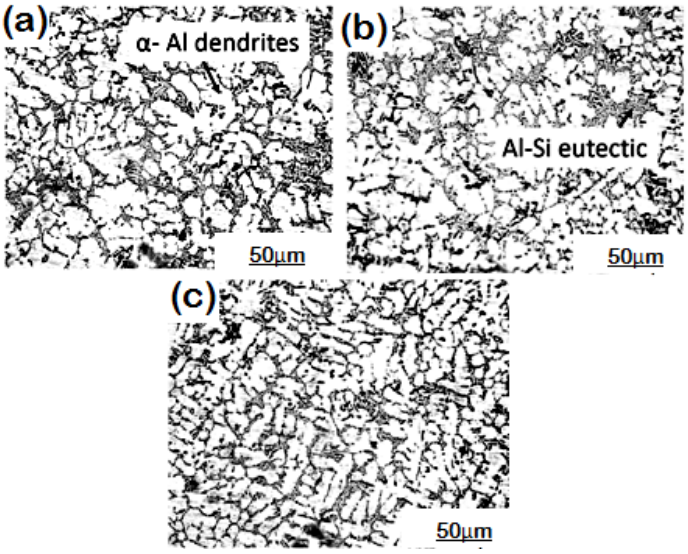

Fig. 4.3 Optical microstructures of a) outer, b) middle and c) inner zone of the radial cross-section of the base A356 alloy

The microstructures of the composite FG -composites (Figs. 4.3-4.9) show predominantly three phases namely, the primary α-Al dendrites, Si eutectic phase, and Mg_2Si. The outer chill zone dendrite arms of α-Al are fragmented due to the centrifugal force similar to the base alloy. The inner zone dendrites are not fragmented; only refined dendrites are observed. So far as the morphology of the Mg_2Si is concerned, two forms of Mg_2Si are discernible, one is the primary blocky type and another one is in the eutectic phase. These eutectic phases of Al-Mg_2Si are formed in the interdendritic regions of α-Al. The eutectic Al-Mg_2Si micro-constituent exhibits the characteristic morphology of ‘‘Chinese script.’’ The phases observed in the as-cast alloy can be explained with the help of Al-Mg-Si phase diagram (Fig. 4.10).

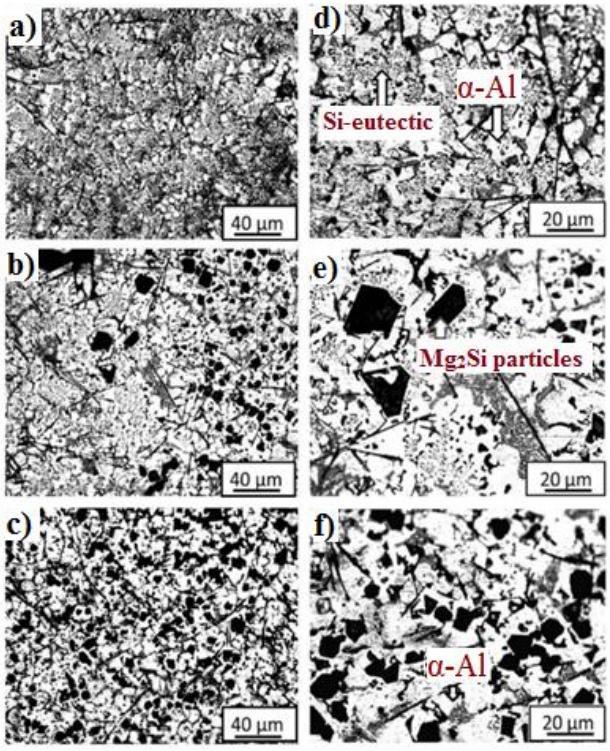

Fig. 4.4 Optical micrographs of a) outer, b) middle and c) inner cross-sectional zones of A356+2.5 Mg FGM and d), e) and f) are corresponding micrographs at higher magnifications

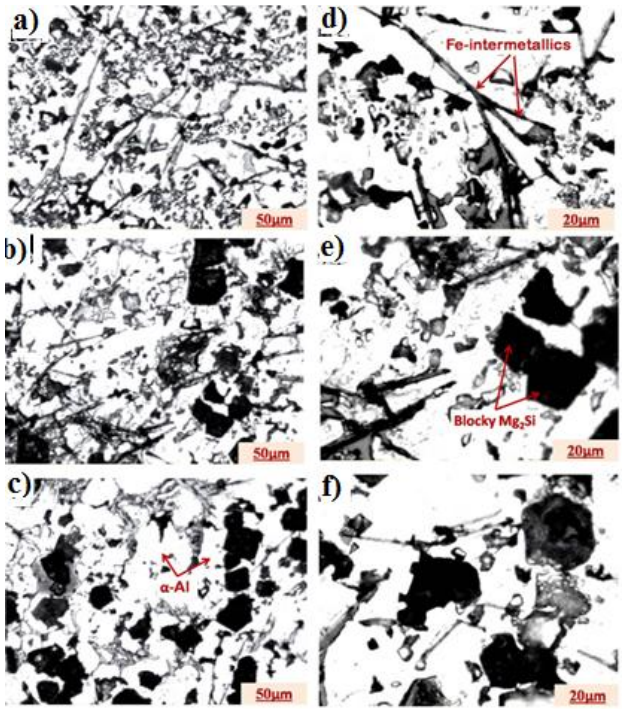

Fig. 4.5 Optical micrographs of a) outer, b) middle and c) inner cross-sectional zones of A356-5 Mg FGM and d), e) and f) are corresponding micrographs at higher magnifications

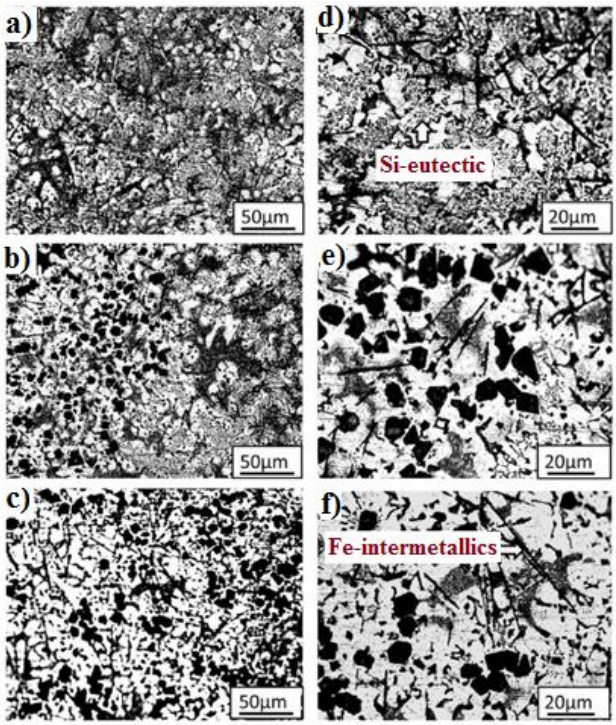

Fig.4.6 Optical micrographs of (a) outer, (b) middle and (c) inner cross-sectional zones of A356-7.5 Mg FGM and (d), (e) and (f) are corresponding micrographs at higher magnifications

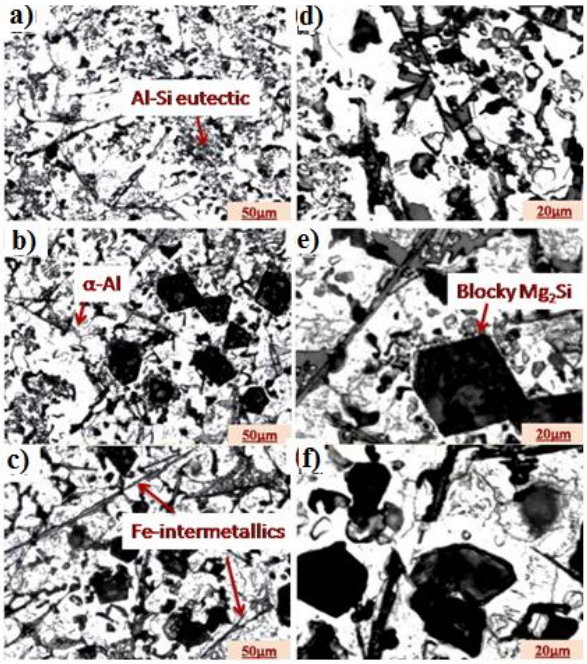

Fig.4.7 Optical micrographs of (a) outer, b) middle and c) inner cross-sectional zones of A356-10Mg FGM and d), e) and f) are corresponding micrographs at higher magnifications

Solidification in the hypoeutectic range commences with the precipitation of primary α-Al within the parent liquid. Progress of solidification below pseudo-eutectic temperature (594^0C) would form proeutectic primary Mg_2Si crystallites within the liquid phase of narrow tri-phase stability area. At the eutectic temperature (583.5^0C), the eutectic Al-Mg2Si is formed from remaining liquid. The reaction can be expressed as,

$$L \rightarrow L_1 + Al \rightarrow L_2 + Al + (Mg_2Si)_p \rightarrow (Mg_2Si)_p + (Al + Mg_2Si)_E$$

where E is a eutectic, P is a primary phase.

On the other hand, the solidification in the hypereutectic range begins with precipitation of primary Mg_2Si crystals. The Mg_2Si particles act as heterogeneous sites for nucleation of α-Al as the solidification progress through tri-phase region forming a layer of α-Al surrounding primary Mg_2Si. Further cooling down below the eutectic temperature, Al + Mg_2Si eutectic is formed as per following reactions:

$$L \rightarrow (Mg_2Si)p + L_1 \rightarrow L_2 + Al + (Mg_2Si)_p \rightarrow (Mg_2Si)_p + (Al + Mg_2Si)_E$$

With increasing extra Mg additions the eutectic reaction point is shifted to lower Mg_2Si content (Fig.4.10b). Thus, excess Mg promotes formation of primary Mg_2Si.

The formation of primary Mg_2Si is also perhaps augmented by the action of centrifugal force. The initial dendrites of Mg_2Si are fragmented and fragmented particles grow in course of movement towards the inner core leading to the formation of blocky Mg_2Si.

The population of primary Mg_2Si particles in the inner zone of the tubes is quite high while in the transition zone the particles are gradually disappearing. However, in the outer zone, a few Mg_2Si particles are observed, as shown in Figs.4.4 to 4.7. The size and volume fraction of primary Mg_2Si particles at different zones are the direct consequence of solidification time or secondary dendritic arm spacing (SDAS). The rapid solidification of molten metal near the mold wall (Table 2) results in the formation numerous nuclei of Mg_2Si particles instantaneously. The nucleation, growth, and transportation depend on the thermal gradient between the mold and the liquid metal poured. The number of nuclei formed in the composites are increasing with increasing Mg wt.%. A large fraction is moved to inner zone provided liquid viscosity permits and centrifugal force is adequate. However, a considerable fraction remained entrapped in the outer zone. The presence of primary Si and Mg_2Si particles have also been observed by other researchers in hypereutectic Al-Si-Mg alloy FGMs [115,116]. Obviously, this fraction is more in A356-7.5 Mg and A356-10Mg FG-composites compared to those in A356-2.5 Mg and A356-5.0Mg as shown in Fig.4.11. As there is no sufficient time for diffusion, the particles are refined of the order of 5-20 μm. The growth of the transported Mg_2Si particles occurs during movement and so long as the inner zone remains liquid. The solidification times at

different zones with varying Mg% are shown in Table 4.2. The solidification time increases as the %Mg is increased and it is expected that the primary Mg_2Si will be coarsened. However, from the size distribution plots of composites (Figs. 4.16 to 4.19), appreciable coarsening of Mg_2Si particles with increasing %Mg is not observed. This is perhaps due to the presence of Fe in the ingot and its refining effect. The increasing percent of Fe in the ingots overshadows the coarsening of Mg_2Si particles. The pronounced effect of Fe on the size and morphology of Mg_2Si in Al-Mg_2Si in-situ composites has been reported by Emamy et al.[117]. The refining effect of Fe is attributed to the poisoning effect i.e. Fe is absorbed in the growth front and restricts the crystal growth.

The secondary dendritic arm spacings were calculated for cast base alloy and FG-composites as shown in Table.4.2. Resultant, the secondary arm spacing are reduced towards the outer zones of tubular cast specimens; because of due to rapid chilling effect at mold wall. The corresponding solidification time is consistently decreases from inner to surface of tubes.

Table.4.2 Secondary dendritic arm spacing (SDAS) and solidification time of base alloy and composite FGMs.

Centrifugally cast (Alloy/FGMs)	Observed Locations	SDAS (±µm)	Solidification Time (Seconds)
A356	Inner	18.17± 0.75	3.75
	Middle	16.44± 0.51	2.77
	Outer	15.04± 0.36	2.12
A356+2.5Mg	Inner	14.98± 0.78	2.09
	Middle	13.75± 0.40	1.62
	Outer	11.46± 0.25	0.94
A356+5.0Mg	Inner	15.50± 0.50	2.32
	Middle	13.57± 0.20	1.56
	Outer	12.46± 0.31	1.21
A356+7.5Mg	Inner	15.73± 0.50	2.43
	Middle	14.02± 0.70	1.72
	Outer	13.42± 0.23	1.51
A356+10.0Mg	Inner	16.01± 0.59	2.56
	Middle	14.50± 0.40	1.90
	Outer	13.45± 0.20	1.52

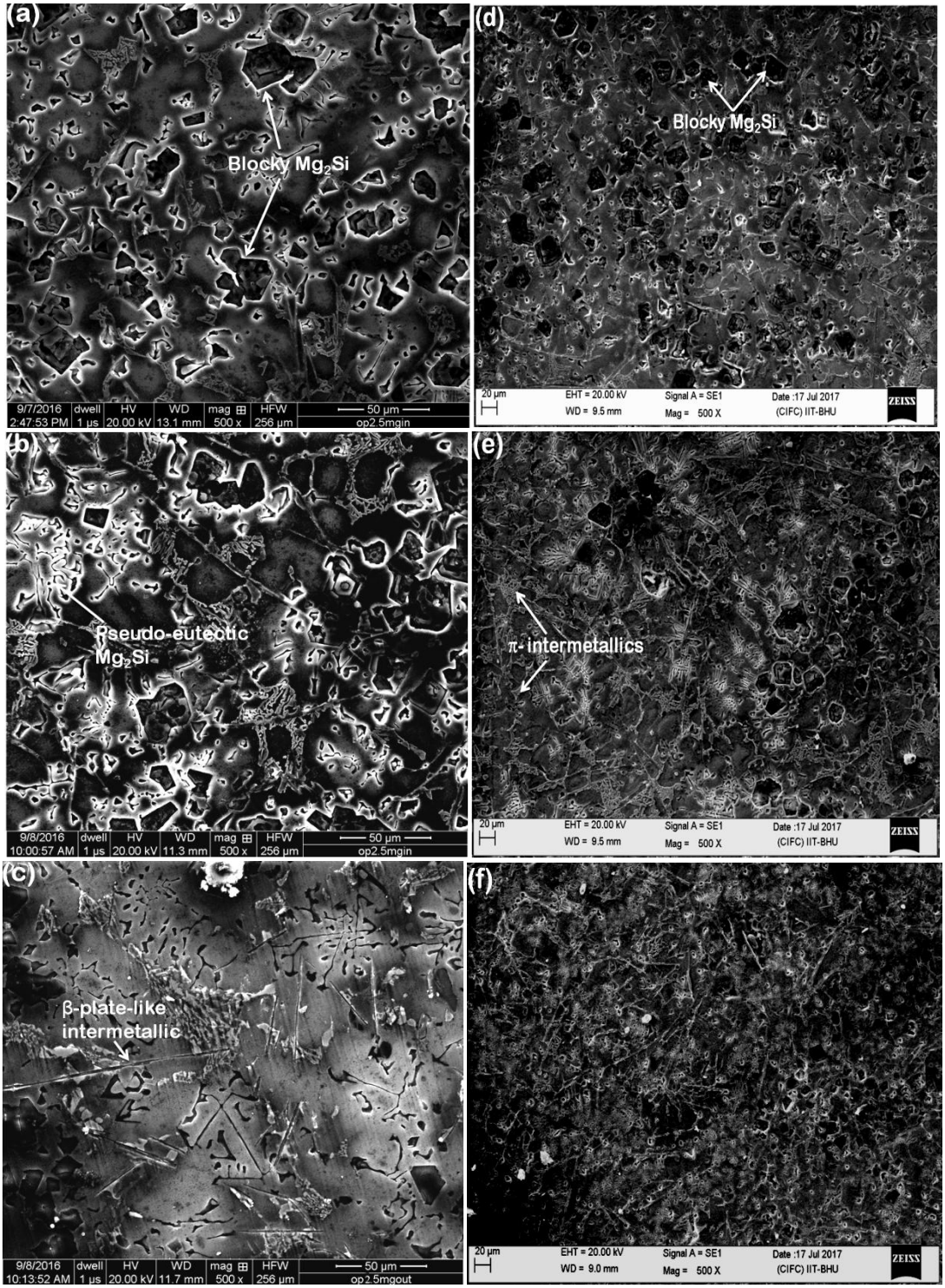

Fig. 4.8 SEM micrographs of a) inner, b) middle, c) outer cross-sectional zones of A356-2.5 Mg FGM and d), e) and f) are corresponding zones of A356-5 Mg FGM respectively

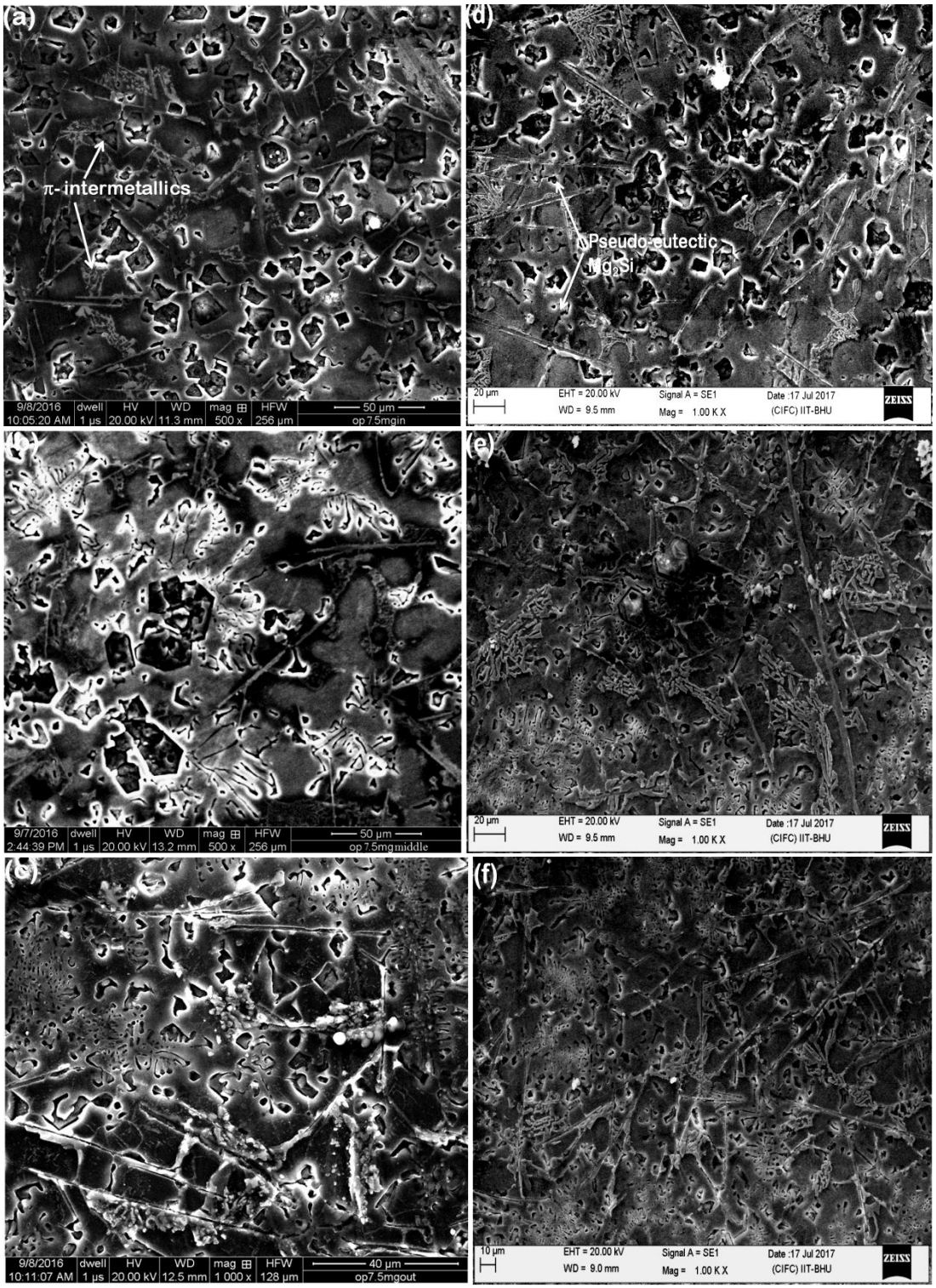

Fig.4.9 SEM micrographs of (a) inner, (b) middle, (c) outer cross-sectional zones of A356-7.5Mg FGM and (d), (e) and (f) are corresponding zones of A356-10 Mg FGM respectively

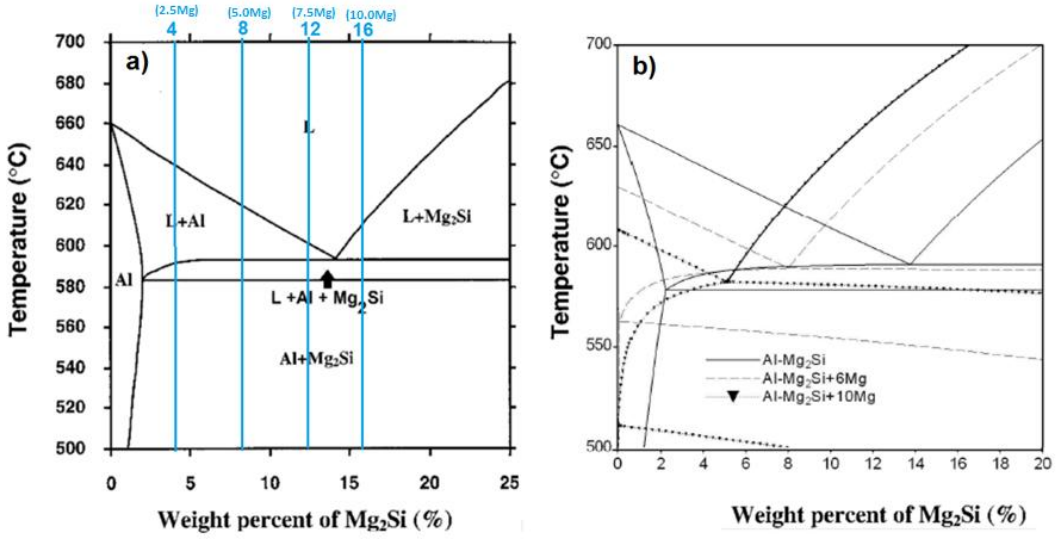

Fig.4.10. a) Equilibrium phase diagrams of the pseudo-binary Al-Mg_2Si [54] and b) Effect of extra addition of Mg on shifting of eutectic point [68].

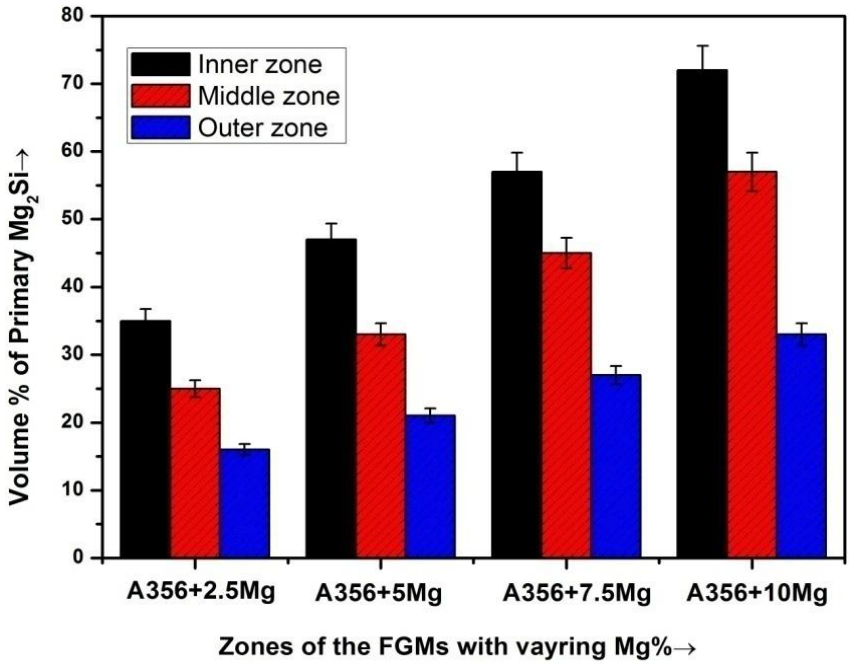

Fig.4.11 Volume % of primary Mg_2Si in different zones of FG composites

4.5 Elemental analysis and size distribution of phases

The elemental mappings by EDS analysis of different elements are shown in Fig. 4.12 to 4.14. From the figures, it is evident that, in middle and outer zones, Si and Mg are distributed almost evenly in all the phases namely α-Al, Al-Mg_2Si eutectic and eutectic Si; however, more preferentially in the primary Mg_2Si and Fe-intermetallics.

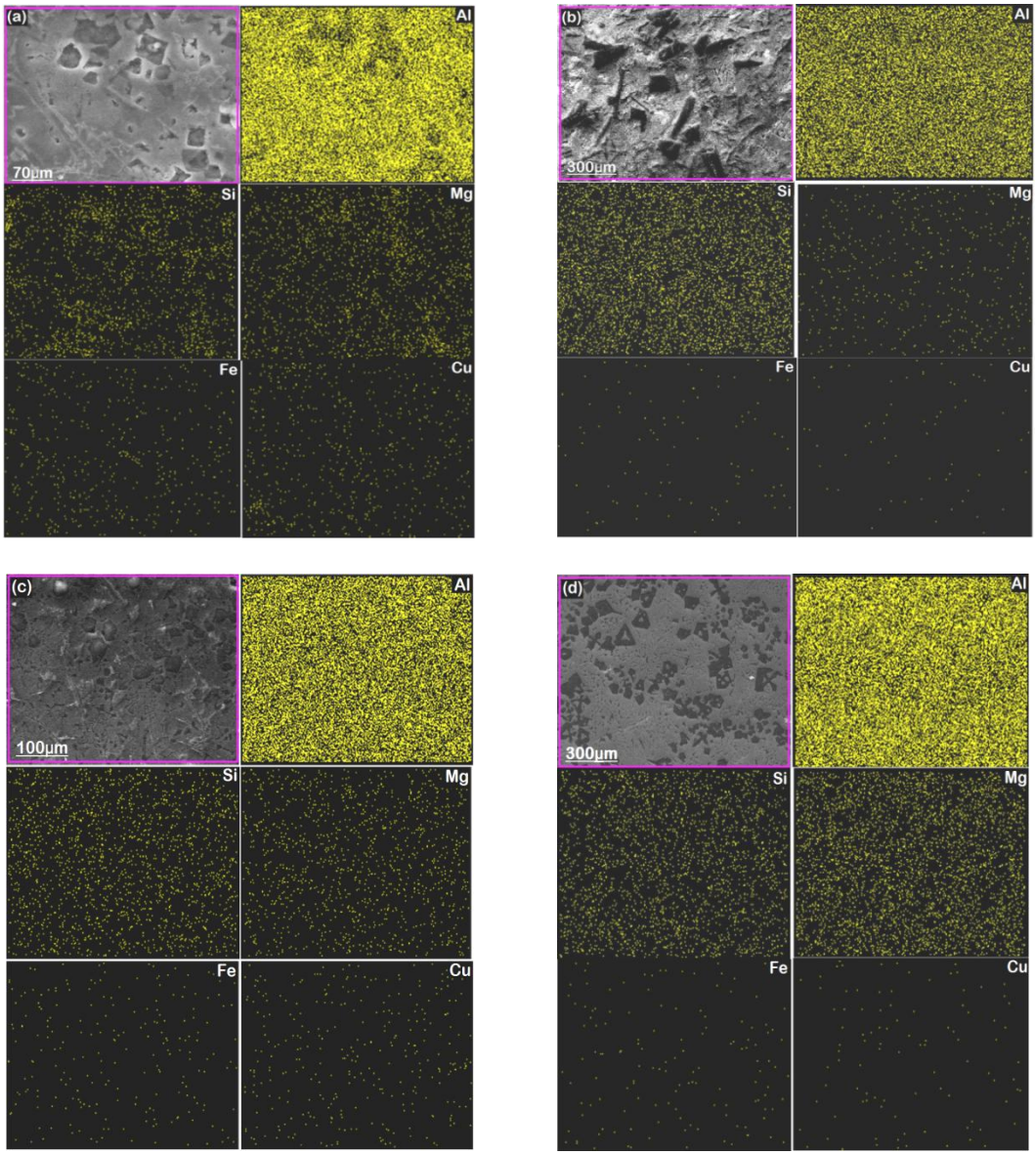

Fig. 4.12 Elemental mappings by EDS analysis of Al, Si, Mg, Fe and Cu in inner zones of(a)A356-2.5Mg and(b) A356-5Mg (c) A356-7.5Mg (d) A356-10Mg FG-composites.

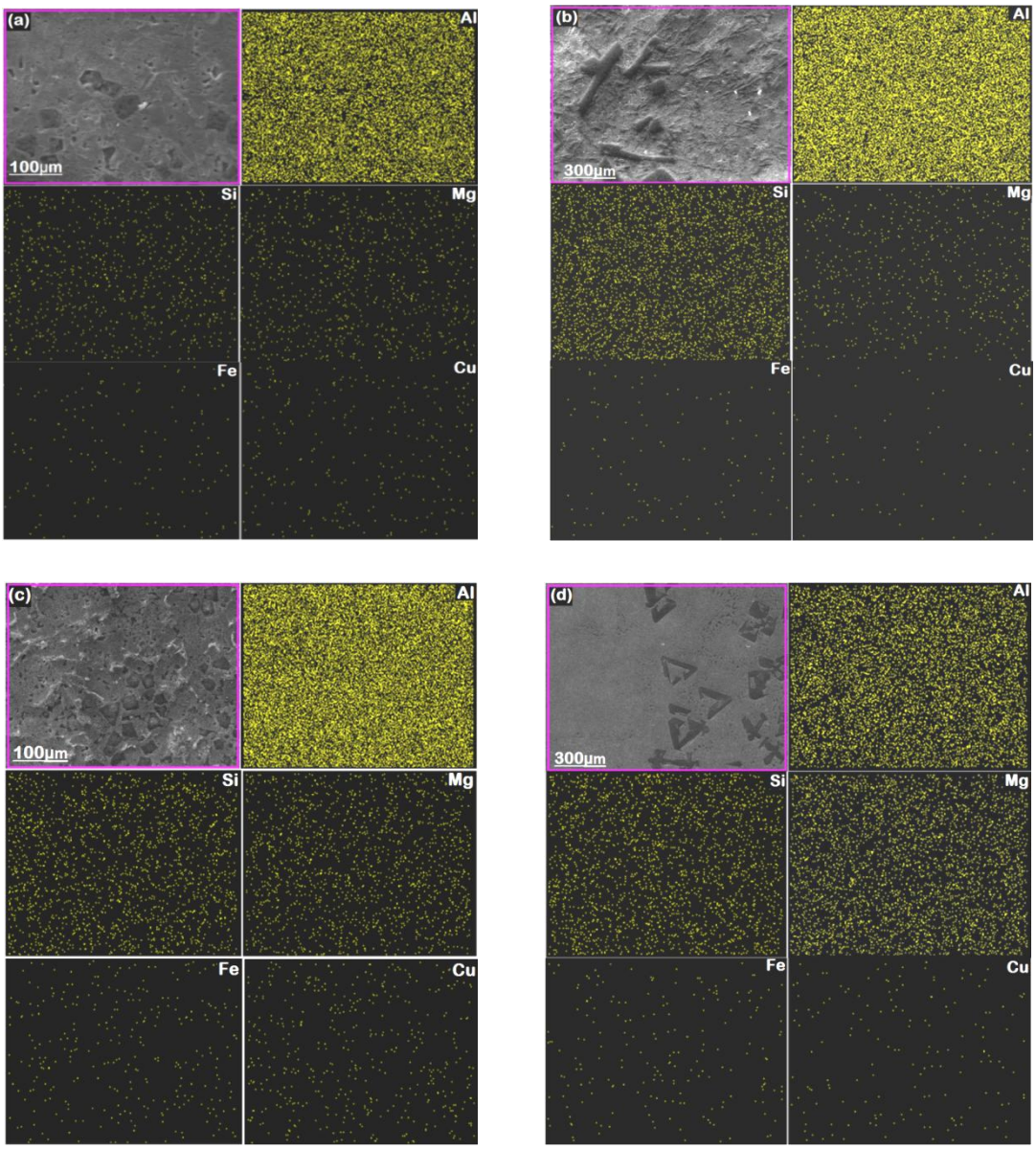

Fig.4.13 Elemental mappings by EDS analysis of Al, Si, Mg, Fe and Cu in middle zones of(a)A356-2.5Mg and(b) A356-5Mg (c) A356-7.5Mg (d) A356-10Mg FG-composites.

A consistent segregation pattern of the reinforcement Mg_2Si must be produced to have a consistent ultimate mechanical property of the tubular liner. Particle segregation area can be controlled by three parameters namely a) pouring temperature of the metal, b) mold temperature and c) G-number; ($G=\omega^2R/g$) where R is the radius of the cast tube (m), ω is the mold rotation crate (in radians s^{-1}) and g is the acceleration due to gravity). With

high pouring temperatures, the viscosity of the melt becomes small and solidification time will be longer; with large G numbers, the velocity of particles is adequate; and with increasing mold temperature the chilling tendency is reduced. As a result, the migration of particles encounters relatively smaller obstacles, and an obviously graded distribution of particle size is formed.

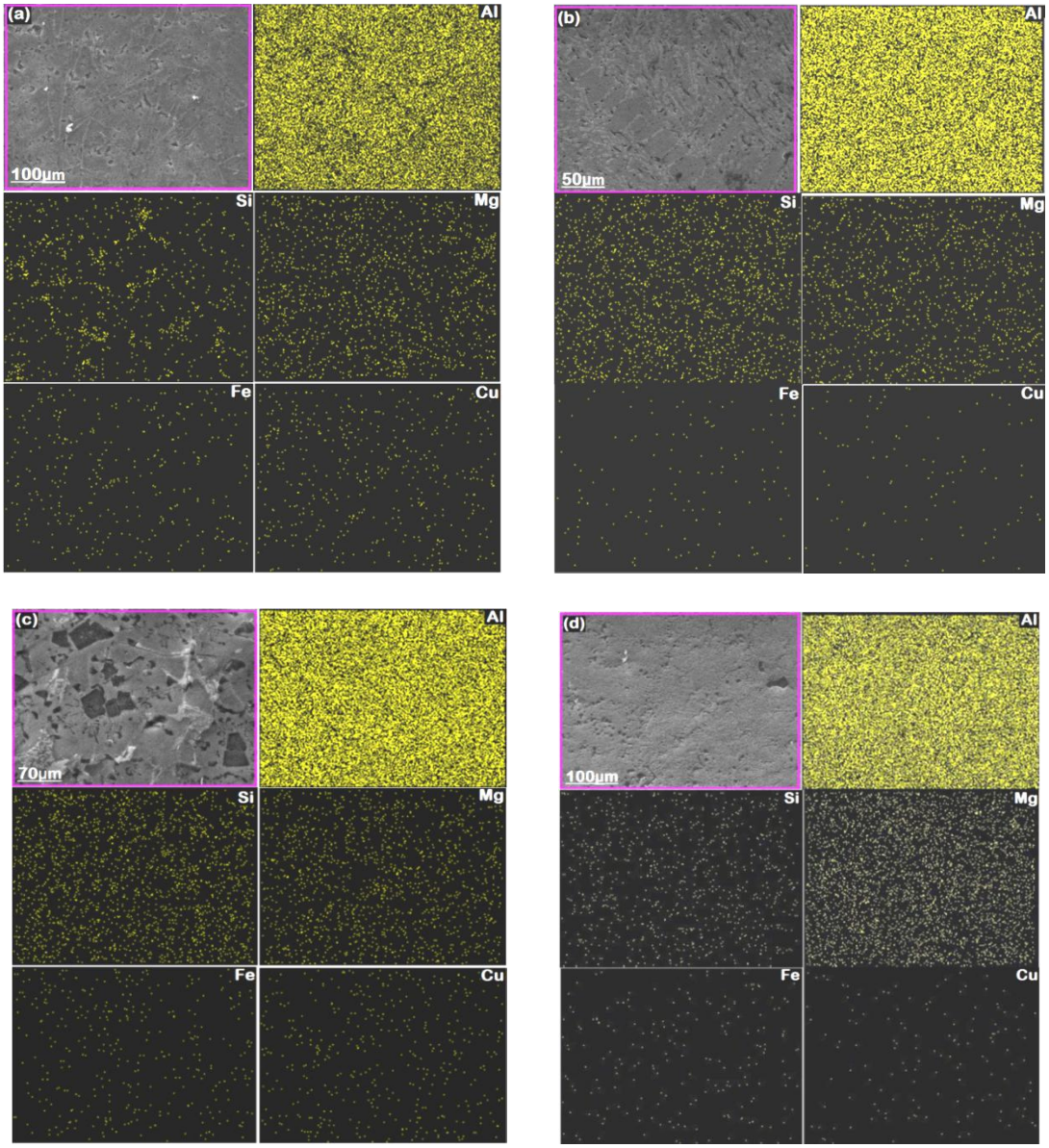

Fig.4.14 Elemental mappings by EDS analysis of Al, Si, Mg, Fe and Cu in outer zones of(a)A356-2.5Mg and(b) A356-5Mg (c) A356-7.5Mg(d) A356-10Mg FG-composites.

Since the solid-state solubility of Fe in Al is very low (max.0.052 wt%), the majority of Fe is expected to be presented in the form of intermetallic compounds. The presence of Fe in the base alloy A356 is responsible for the formation of Al-Fe-Si intermetallic phase in the composites (Figs.4.6-4.9) which is frequently present as a blade- or plate-shaped [118]. Blade-like intermetallic phases in Al-Si alloys are identified as β-Al_5FeSi [119-121]. The length of these phases is observed to be several tens of microns crossing the eutectic Al-Si clusters, while their thickness is of the order of 0.5 mm. With an increase in Mg % another type of Al-Fe-Mg-Si intermetallic is formed called π-$Al_8FeMg_3Si_6$ having Chinese script morphology (Fig. 4.15). The Fe-rich intermetallic observed in A356-2.5%Mg and A356-5.0Mg FG-composites is mostly β-phase whereas the higher quantities of π-phase particles is observed in A356-7.5%Mg and A356-10.0Mg FG-composites. Two possible reaction routes for π-phase formation are;

- by peritectic reaction which transforms β-phase into π-phase,

$$L\ (Al\text{-}Mg\text{-}Si\ soln.) + (\beta)Al_5FeSi \rightarrow Al\text{-}Si + (\pi)Al_8Mg_3FeSi_6$$

- by quaternary eutectic reaction at the end of solidification sequence,

$$L\ (Al\text{-}Mg\text{-}Si\ soln.) \rightarrow Al\text{-}Si + Mg_2Si + (\pi)Al_8Mg_3FeSi_6.$$

The π-phase intermetallics are observed to be in close contact with β-platelets, and their interfaces are seamlessly fused. This is probably due to the growth of π-phase from the surface of initial β-phase by peritectic reaction [122].

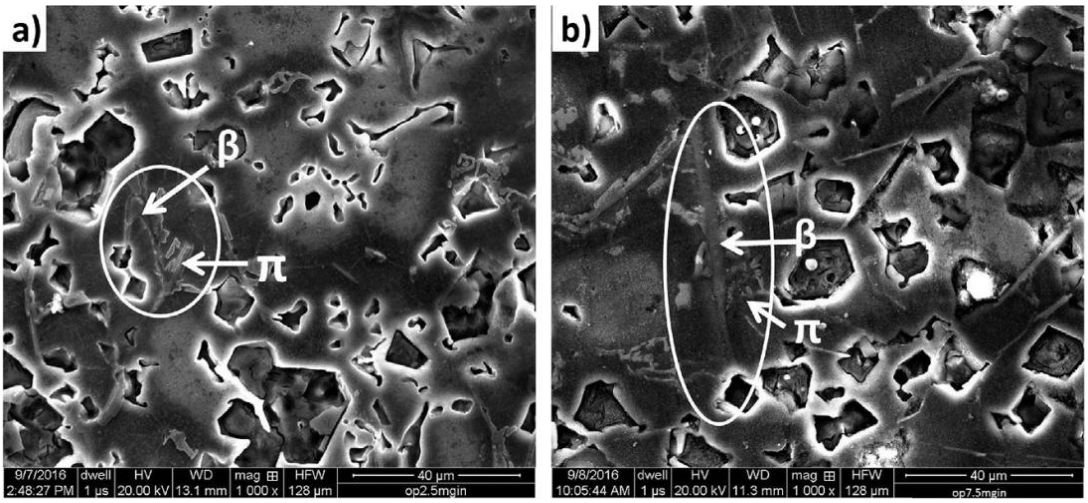

Fig. 4.15 π-intermetallics close to plate-like β-intermetallics in inner zone A356-7.5Mg FG composites.

Increasing the Fe content will increase the quantity and size of the β-phase in the microstructure. The average sizes of these intermetallics are dependent on the cooling rate or the SDAS. With higher cooling rate near the outer zone, the sizes are finer and have a gradual tendency to increase towards the inner zone (Figs.4.16 and 4.19). This chilling refining tendency is more prominent with higher Mg content, more numbers of intermetallic nuclei are formed but the growth is restricted. This is in agreement with the findings of Caceres et al. [123]. The total volume fraction of the Al-Fe-Si intermetallic (i.e. β and π-phases) has been found to increase with increase in wt.% Mg and Fe in the A356-7.5% Mg and A356-10.0%Mg FG-composites (Fig. 4.20).

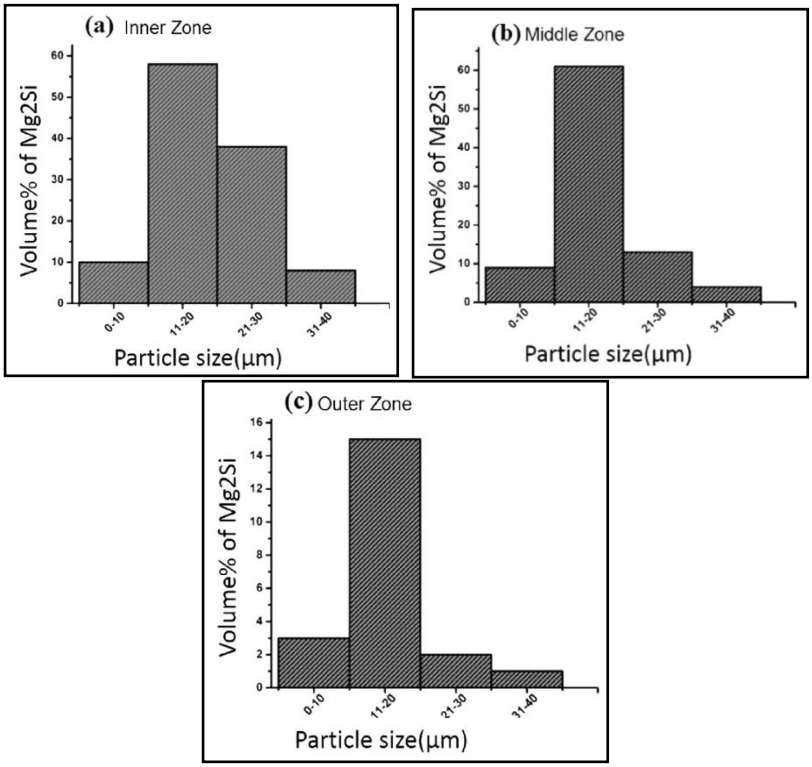

Fig.4.16 Size distribution of Mg_2Si particles in different zones of A356-2.5 %Mg FGM composite

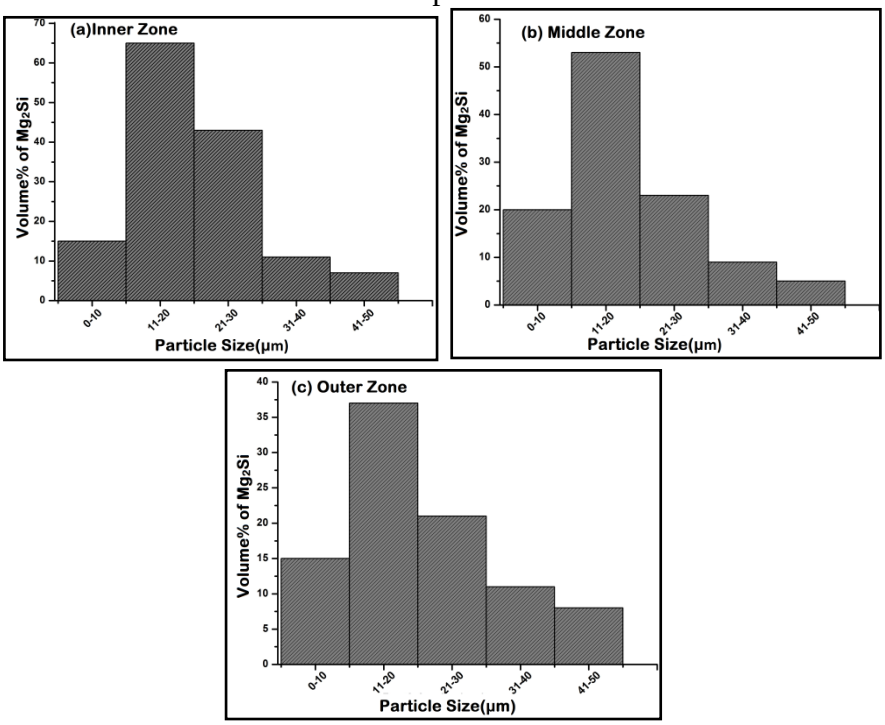

Fig.4.17 Size distribution of Mg_2Si particles in different zones of A356-5 %Mg FGM composite

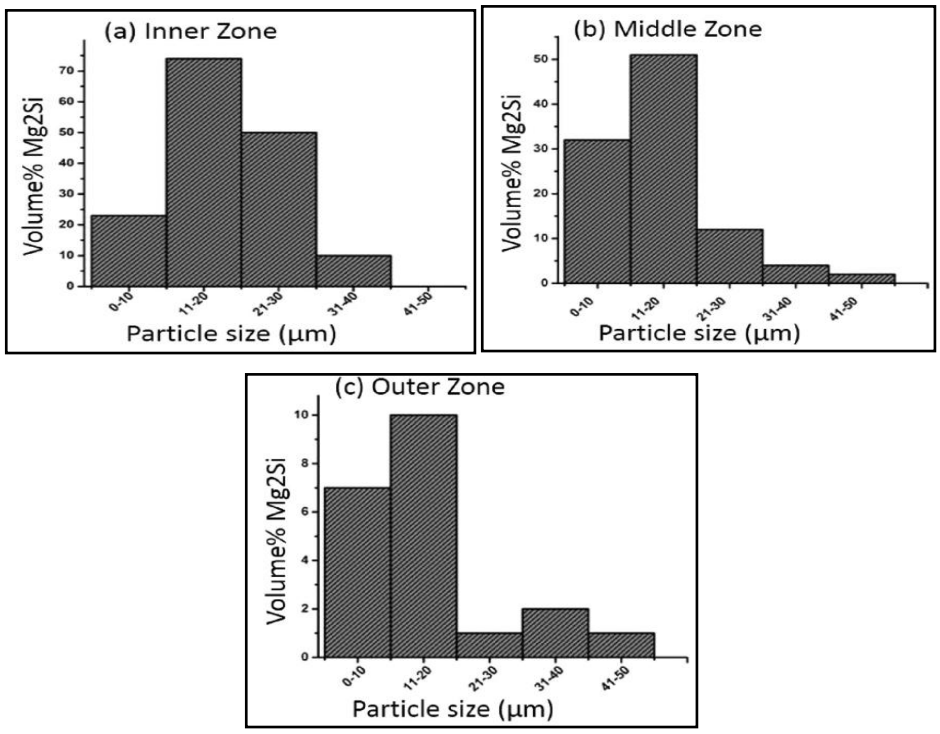

Fig.4.18 Size distribution of Mg_2Si particles in different zones of A356-7.5 %Mg FGM

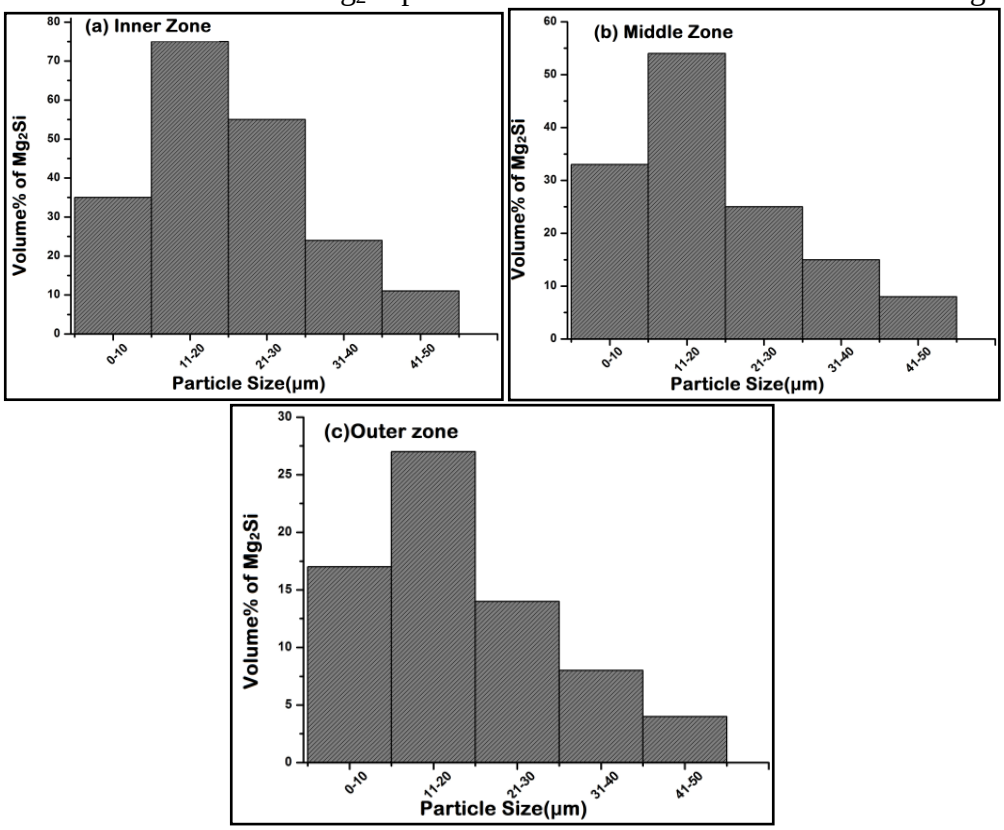

Fig.4.19 Size distribution of Mg_2Si particles in different zones of A356-10%Mg FGM

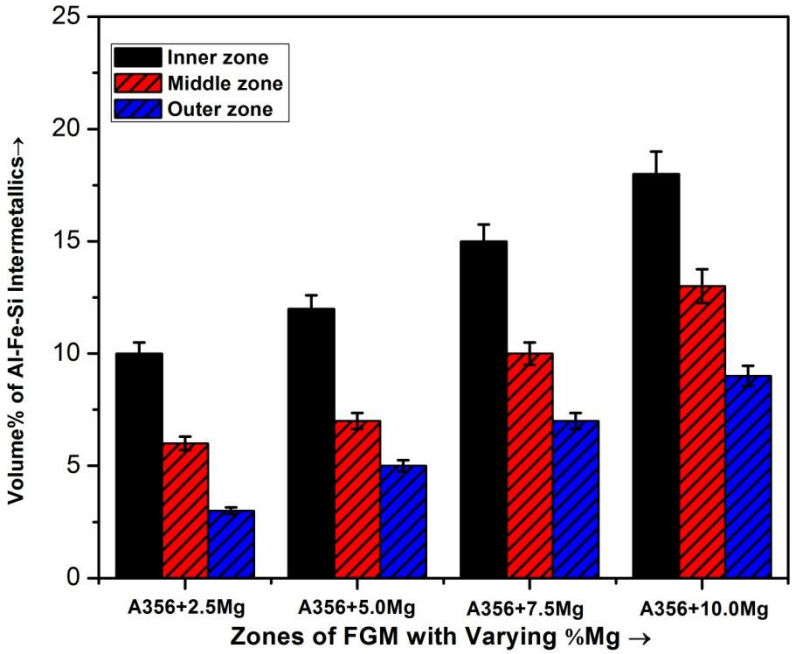

Fig.4.20 Volume % of Al-Fe-Si intermetallic in different zones of FG composites

Transmission Electron Micrographs have been shown in Figs.4.21 to 4.22. The morphologies of the Mg_2Si reinforcements and matrix structures are clearly seen in the figures. The primary Mg_2Si have the shape of truncated octahedron and the eutectic Mg_2Si are of rod-shapes. The in-situ formed Mg_2Si reinforcements are defect free and particle/matrix interfaces are clear which would result in good interfacial bond strength. The ultimate properties are dictated by this interfacial bond strength. The matrix structures show dislocations due to strain fields created surrounding the Mg_2Si particles. The strain fields are developed due to the mismatch in the co-efficient of thermal expansion between the matrix and the Mg_2Si in course of solidification (coefficient of thermal expansion of Mg_2Si is $7.5x10^{-6}\ K^{-1}$and that of A356 alloy is $23.4\ x10^{-6}\ K^{-1}$).

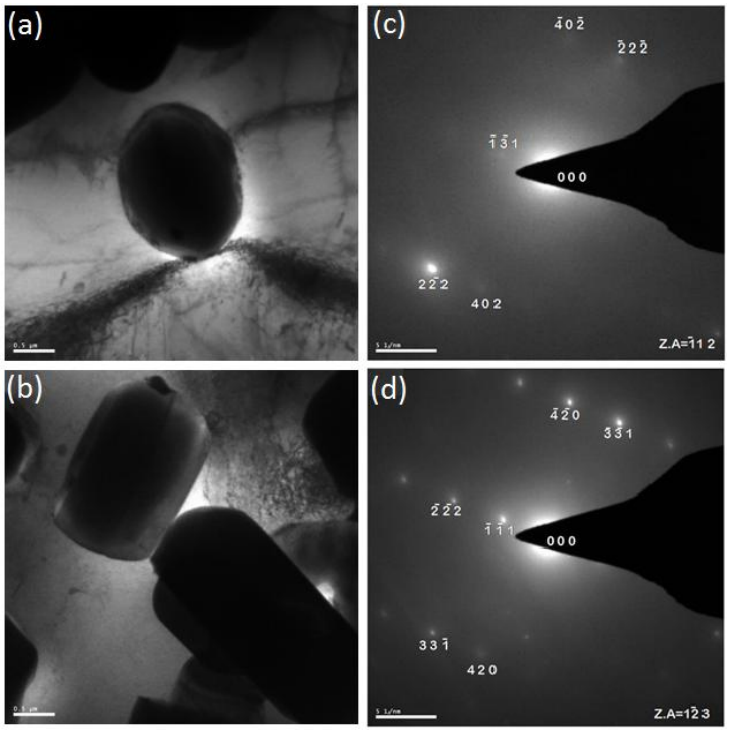

Fig.4.21. Bright field TEM image of inner layer of A356-2.5%Mg FG composite; a) ,b) showing different morphologies of Mg_2Si particles in matrix with dislocations; c) and d) are corresponding SAD patterns of Mg_2Si particle and matrix respectively.

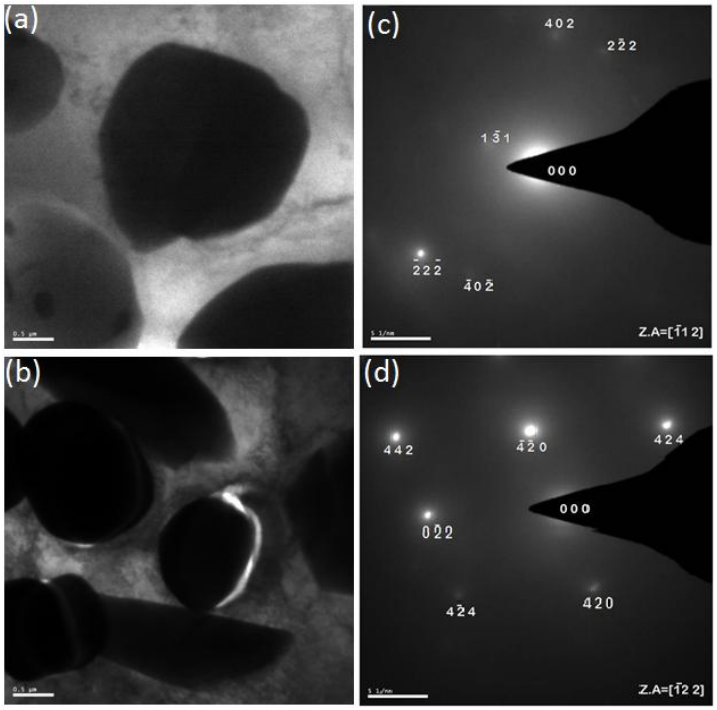

Fig.4.22.Bright field TEM image of inner layer of A356-7.5%Mg FG composite; a), b) showing different morphologies of Mg_2Si particles in matrix with dislocations; c) and d) are corresponding SAD patterns of Mg_2Si particle and matrix respectively.

4.6. Determination of average %porosity

The %porosities of all fabricated FGMs were calculated, by Archimedes principle as shown in Table.4.3. The theoretical density values were measured by applying the rule of

Table.4.3. Density and Porosity% with increasing Mg wt.%.

FG-Composites	Cross-section	Theoretical Density of composite (ρ_{th}) ($\rho_c=v_f*\rho_f+v_m*\rho_m$)	Experimental Density of composite (ρ_{exp})	Volume Fraction of particles (v_f)	Volume Fraction of Matrix (v_m)	Porosity (%) $=\frac{\rho_{exp}-\rho_{th}}{\rho_{th}}$	Average Porosity(%)
A356+ 2.5Mg	Inner zone	2.51	2.60	0.27	0.73	3.58	3.86
		2.48	2.60	0.30	0.70	4.84	
		2.52	2.60	0.25	0.75	3.17	
	Middle zone	2.56	2.65	0.19	0.81	3.52	3.78
		2.55	2.65	0.20	0.80	3.92	
		2.55	2.65	0.21	0.79	3.92	
	Outer Zone	2.54	2.63	0.22	0.78	3.54	3.13
		2.55	2.63	0.21	0.79	3.13	
		2.56	2.63	0.20	0.80	2.73	
A356+ 5.0Mg	Inner zone	2.45	2.58	0.35	0.65	5.31	5.72
		2.44	2.58	0.37	0.63	5.71	
		2.43	2.58	0.38	0.62	6.16	
	Middle zone	2.44	2.56	0.33	0.67	4.91	4.49
		2.45	2.56	0.35	0.65	4.49	
		2.46	2.56	0.32	0.68	4.06	
	Outer zone	2.50	2.59	0.25	0.75	3.60	3.46
		2.51	2.59	0.27	0.73	3.18	
		2.50	2.59	0.24	0.76	3.60	
A356+ 7.5Mg	Inner zone	2.40	2.57	0.43	0.57	7.08	6.20
		2.43	2.57	0.37	0.63	5.77	
		2.43	2.57	0.38	0.62	5.76	
	Middle zone	2.48	2.61	0.30	0.70	5.24	5.67
		2.46	2.61	0.31	0.69	6.10	
		2.47	2.61	0.33	0.67	5.67	
	Outer zone	2.49	2..58	0.30	0.70	3.61	4.31
		2.47	2.58	0.31	0.69	4.45	
		2.46	2.58	0.33	0.67	4.87	
A356+ 10.0Mg	Inner zone	2.34	2.55	0.45	0.55	8.97	7.45
		2.38	2.55	0.42	0.58	7.14	
		2.40	2.55	0.39	0.61	6.25	
	Middle zone	2.41	2.57	0.41	0.59	6.68	6.47
		2.42	2.57	0.40	0.60	6.36	
		2.42	2.57	0.39	0.61	6.36	
	Outer zone	2.43	2.56	0.38	0.62	5.34	5.58
		2.40	2.56	0.39	0.61	6.47	
		2.44	2.56	0.37	0.63	4.92	

With increasing Mg content, the density of the composites marginally decreases as the volume% blocky Mg_2Si increases and Mg_2Si has lower density compared to the base alloy A356. So far as the porosity is concerned, FG-composites are prone to have higher porosity due to its relatively long freezing range. So, higher the Mg content, higher will be the %porosity resulting in further reduction in the density. Higher %porosities are observed in the inner zones of all %Mg and these are decreasing towards the outer zones due to variation in solidification time.

4.7.Chapter summary

The effect of varying Mg content on in-situ A356-Mg_2Si composite functionally graded material have been investigated. From the analysis of the results, the following conclusions can be drawn:

I. The microstructure of centrifugally cast Al-Si-Mg alloy base in-situ composites consist of mainly four phases such as, α-Al, Al-Si eutectic, Al-Mg_2Si pseudo-eutectic and primary blocky Mg_2Si. The primary Mg_2Si have a shape of truncated octahedron. Apart from these phases, Fe forms blade-shaped Al-Fe-Si intermetallic.

II. The blocky primary Mg_2Si particles are predominantly segregated at the inner layer of the centrifugally cast tubes due to the relative density effect with respect to molten Al. Ultimately after solidification, three distinct zones are formed in the radial direction of cross-section viz. highly particle populated inner zone, and gradually particle-depleted middle transition zone and the outer zone. This distribution gives rise to a functionally graded composite. However, a minor quantity of Mg_2Si particle remains entrapped in the outer zone due to rapid cooling rate.

III. The solidification time is most rapid at the outer zone due to sudden chilling and SDAS are the finest which gradually become coarser towards the inner zone because of slower cooling rate. The Mg_2Si particles are refined due to finer SDAS. Since the cooling rate in the inner zone is slower the volume% of Fe-intermetallic is higher.

IV. Dislocations in the matrix surrounding Mg_2Si particles are observed generated during solidification due to mismatch in co-efficient thermal expansion of Mg_2Si and the matrix.

V. With increasing %Mg, the porosity% is increasing due to longer freezing range. Porosities are minimum at the outer zones and gradually increasing towards the inner zones because of the effect of solidification time; inner zones are solidifying last.